Co/Ba/La_2O_3 catalyst for ammonia synthesis under mild reaction conditions

Shin-ichiro Miyahara,[a] Katsutoshi Sato,*[a,b] Yuta Ogura,[a] Kotoko Tsujimaru,[c] Yuichiro Wada,[c] Takaaki Toriyama,[d] Tomokazu Yamamoto,[e] Syo Matsumura,[d,e] Koji Inazu,[f] and Katsutoshi Nagaoka*[a]

---

[a] Department of Chemical Systems Engineering, Graduate school of Engineering, Nagoya University, Furo-cho, Chikusa-ku, Nagoya, 464-8603, Japan

[b] Elements Strategy Initiative for Catalysts and Batteries, Kyoto University, 1-30 Goryo-Ohara, Nishikyo-ku, Kyoto, 615-8245, Japan

[c] Department of Integrated Science and Technology, Faculty of Science and Engineering, Oita University, 700 Dannoharu, Oita, 870–1192, Japan

[d] The Ultramicroscopy Research Center, Kyushu University, Motooka 744, Nishi-ku, Fukuoka, 819- 0395, Japan

[e] Department of Applied Quantum Physics and Nuclear Engineering, Kyushu University, Motooka 744, Nishi-ku, Fukuoka, 819-0395, Japan

[f] National Institute of Technology, Numazu College, 3600 Ooka, Numazu, Shizuoka, 410-8501, Japan

***Corresponding authors**

K. Sato: sato.katsutoshi@marerial.nagoya-u.ac.jp

K. Nagaoka: nagaoka.katsutoshi@material.nagoya-u.ac.jp

Abstract

Ruthenium catalysts may allow realization of renewable energy–based ammonia synthesis processes using mild reaction conditions (<400 °C, <10 MPa). However, ruthenium is relatively rare and therefore expensive. Here, we report a Co nanoparticle catalyst loaded on a basic Ba/La_2O_3 support and pre-reduced at 700 °C ($Co/Ba/La_2O_3$_700red) that showed higher ammonia synthesis activity at 350 °C and 1.0–3.0 MPa than two benchmark Ru catalysts, Cs^+/Ru/MgO and Ru/CeO_2. The synthesis rate of the catalyst at 350 °C and 1.0 MPa (19.3 mmol $h^{-1}g^{-1}$) was 8.0 times that of $Co/Ba/La_2O_3$_500red and 6.9 times that of Co/La_2O_3_700red. The catalyst showed activity at temperatures down to 200 °C. High-temperature reduction induced formation of a BaO-La_2O_3 nano-fraction around the Co nanoparticles, which increased turnover frequency, inhibited Co nanoparticle sintering, and suppressed ammonia poisoning. These strategies may also be appliable to nickel catalysts.

Keywords: renewable energy, hydrogen carrier, ammonia fuel, heterogeneous catalysis, Co catalyst

1. Introduction

Ammonia (NH_3) is an essential chemical feedstock in the modern chemical industry. More than 80% of the ammonia generated today is used as chemical fertilizer, and ammonia has made a huge contribution to solving the food crisis that resulted from the population explosion in the 20th century [1-3]. Recently, ammonia has attracted attention as a hydrogen and energy carrier for greater utilization of renewable energy, and as a decarbonized fuel for use in power plants and ships [4-7]. Ammonia, therefore, is considered an important material for realizing a sustainable society.

Traditionally, ammonia has been produced via the Haber–Bosch process. The Haber–Bosch process uses very high pressures and temperatures (>450 °C and >20 MPa) and has been highly optimized from a process engineering standpoint. However, the process uses fossil fuels as its source of hydrogen, and therefore it emits large amounts of CO_2 (1.9 ton-NH_3^{-1}) to the atmosphere [8]. If ammonia could be produced from hydrogen produced by renewable energy, the process could be harnessed to speed up decarbonization, slow down global warming, and increase food production, which are three important current global issues [9]. A major milestone in the realization of green ammonia synthesis systems using H_2 produced by renewable energy is the development of catalysts that have high ammonia activity under mild conditions (<400 °C, <10 MPa).

The catalysts most commonly used in the Haber–Bosch process are Fe-based; however, these catalysts require a high temperature and pressure to dissociate the N≡N triple bond (945 kJ mol^{-1}) and so are not suitable for use in conjunction with renewable energy [10-13]. In contrast, Ru catalysts show unparalleled ammonia synthesis activity under mild conditions [14-30], but Ru is a rather rare element that is expensive to procure. Co is cheaper and more abundant than Ru, but neat Co is less active than both Ru and Fe because the N_2 molecular adsorption energy of Co is lower than that of Ru and Fe [31]. As a result, previously reported oxide- or carbon-supported Co

catalysts, which have the advantage of being easy to prepare and handle, all show low ammonia synthesis activity under mild conditions [32-34].

As part of efforts to address this issue, we previously reported that the addition of Ba to Co/MgO and pre-reduction at high temperature markedly improved the ammonia synthesis activity of the parent catalyst under mild reaction conditions (<400 °C, 1–3 MPa) [35]. In fact, the resultant Co@BaO/MgO catalyst, where the Co core is encapsulated by a strongly basic BaO shell, showed an activity that was not only higher than that of other oxide- or carbon-supported Co-based catalysts, but also higher than that of active Ru catalysts such as $Ru/La_{0.5}Ce_{0.5}O_{1.75}$ and Cs-Ru/MgO [16,35]. Characterization of our catalyst revealed that the structure allows for exceptional electron donation from BaO via Co atoms to the antibonding π-orbital of N_2 molecules, thereby promoting cleavage of the N≡N bond. Our findings prompted us to examine the use of other basic oxide supports, such as La_2O_3, which has a higher basicity than does MgO [36,37].

Here, we report that $Co/Ba/La_2O_3$ pre-reduced at 700 °C showed high ammonia synthesis rates at a low reaction temperature of 350 °C: 19.3 mmol $h^{-1}g^{-1}$ at 1.0 MPa and 35.7 mmol $h^{-1}g^{-1}$ at 3.0 MPa. Investigations revealed that addition of Ba and increasing the pre-reduction temperature from 500 to 700 °C increased the ammonia synthesis activity by 6.9 and 8 times, respectively, via the formation of a core (Co) - shell ($BaO\text{-}La_2O_3$) structure. The presence of BaO retarded sintering of the Co nanoparticles during high-temperature reduction. The ammonia synthesis activity–promoting effects of the addition of Ba and of increasing the reduction temperature were observed also for Ni catalysts, for which the N_2 adsorption energy of neat Ni is less than that of Co [35]. To further understand how the addition of Ba and the increase of reduction temperature affected the ammonia synthesis rate, X-ray absorption fine structure spectroscopy (XAFS), spherical aberration-corrected scanning transmission electron microscopy (Cs-STEM), and energy electron loss spectroscopy (EELS) analyses were performed on pre-reduced catalyst without exposure to air. In the present study, both EELS and energy-dispersive X-ray (EDX) spectrometry were used;

however, EELS can distinguish between Ba and La elements, whereas EDX spectrometry cannot because in that technique the excitation wavelength of Ba and La are so similar that the small peak attributable to Ba overlaps the large peak attributable to La.

2. Experimental section

2.1. Catalyst preparation

The Ba/La_2O_3 support was prepared by a precipitation and impregnation method as follows. First. a suspension of La hydroxides was formed by dropping an aqueous solution of $La(NO_3)_3 \cdot 6H_2O$ (Wako Pure Chemical, Japan) into a 28 wt% solution of aqueous ammonia (Wako Pure Chemical). The La hydroxides were collected by filtration, washed with distilled water, and added to an aqueous solution containing $Ba(OH)_2 \cdot 8H_2O$ (Wako Pure Chemical). After stirring the suspension for 1 h, the aqueous solvent was removed by rotary evaporation. The resulting powder was calcined at 700 °C in static air and used as the catalyst support.

Next, Co was loaded onto the support. Bis(2,4-pentanedionate)cobalt(II) dihydrate (Tokyo Chemical Industry, Japan) dissolved in tetrahydrofuran (Wako Pure Chemical) was used as the Co precursor. The support was added to the dissolved in the precursor and the suspension was stirred overnight. When the stirring was finished, the tetrahydrofuran was removed by rotary evaporation, leaving behind a powder that was then heated to 500 °C under an Ar flow. The Co loading was fixed at 20 wt% for each catalyst. Two benchmark Ru catalysts (Ru/CeO_2 and $Cs^+/Ru/MgO$) were also prepared as we reported previously [14,37].

2.2. Ammonia synthesis activity test

The rate of ammonia synthesis over the catalysts was measured by using 100 mg of catalyst and a conventional flow system with tubular reactor under either atmospheric pressure or high pressure, as reported previously [38]. Research-grade gases (>99.99%) were supplied from high-

pressure cylinders and purified with a gas purifier (Micro Torr MC50-904FV, SAES Pure Gas, US). The catalysts were pre-reduced *in situ* with pure H_2 (60 mL min^{-1}) at 500, 700, or 800 °C for 1 h at 0.1 MPa and then cooled at 300 °C in an Ar stream. The pressure was then adjusted to 0.1, 1.0, or 3.0 MPa. A mixture of N_2 (30 mL min^{-1}) and H_2 (90 mL min^{-1}) was then passed over the catalyst (space velocity = 72,000 mL h^{-1} g^{-1}). The produced ammonia gas was trapped in an aqueous solution of H_2SO_4, and the rate of ammonia synthesis was calculated from the decrease in the electron conductivity of the H_2SO_4 aqueous solution, which was monitored with an electron conductivity detector (CM-30R, DKK-TOA, Japan).

2.3. Kinetic analysis

Reaction kinetics were analyzed as previously reported [35,39,40]. The reaction orders with respect to N_2, H_2, and NH_3 were calculated by measuring the N_2, H_2, and NH_3 pressure dependence of the NH_3 synthesis rate and by assuming that the rate of the reaction (r) could be described by the following expression:

$$r = kP_{N_2}^{n} P_{H_2}^{h} P_{NH_3}^{a}$$

2.4. Characterization

High-angle annular dark-field scanning transmission electron microscope (HAADF-STEM) images, EDX elemental maps, and EELS spectra were obtained with an aberration-corrected electron microscope (JEM-ARM200CF, JEOL, Japan). The scanning transmission electron microscopy observations were conducted at 120 kV to reduce damage to the sample by the electron beam. Catalyst samples were pre-reduced at 500 or 700 °C under a H_2 flow and then crushed and powdered. Samples of the powdered catalyst were then placed on transmission electron microscopy grids in a glovebox. The grids were then transferred by means of a special holder with a gas cell from the glovebox to the inside of the transmission electron microscopy

column without being exposed to air. For the other observations, samples were dispersed in ethanol under ambient conditions, and samples of the dispersion were dropped onto a carbon-coated copper grid and dried under a vacuum at ambient temperature for 24 h.

The specific surface area of the catalysts was measured by using the Brunauer–Emmett–Teller method. Test samples were pretreated at 300 °C in a vacuum, and the amount of N_2 adsorbed was measured with a BELSORP-mini gas adsorption instrument (BEL Japan, Inc., Japan).

H_2 chemisorption capacity was measured with a BELCAT-B apparatus (MicrotracBEL, Japan). H_2 was fed to a 100-mg sample of catalyst at 60 mL min^{-1}, and the temperature was increased at a rate of 10 °C min^{-1} from room temperature to 500, 700, or 800 °C. The sample was maintained at the desired temperature for 60 min in the H_2 flow; it was then purged with a stream of Ar (60 mL min^{-1}) for 30 min, cooled to 35 °C, and flushed with Ar for 60 min. After pretreatment, H_2 chemisorption measurement was carried out at 35 °C.

XAFS measurements of the Co K-edges were performed on the B01B1 beamline at Spring-8(Hyogo, Japan) with the approval of the Japan Synchrotron Radiation Research Institute (Hyogo, Japan).

X-ray diffraction (XRD) analysis was performed with a SmartLab X-ray diffractometer (Rigaku, Japan) equipped with a CuKα radiation source. The XRD patterns were analyzed by using the PDXL2 software (Rigaku) and three databases (International Centre for Diffraction Data database, Crystallography Open Database, and AtomWork database).

Temperature-programmed reduction measurements were performed under a flow of 100% H_2 using a BEL-CAT-II apparatus (MicrotracBEL). The flow rate of the gas was 60 mL min^{-1}. A 100-mg sample of catalyst was heated from 25 to 1000 °C at a rate of 10 °C min^{-1}. The CH_4, H_2O, CO, and CO_2 profiles were monitored by a quadruple mass spectrometer at m/e =16, 18, 28, and 44, respectively.

3. Results and Discussion

3.1. Ammonia synthesis activity

First, we examined the influence of reduction temperature (500–800 °C) on the NH_3 synthesis rate of the $Co/Ba/La_2O_3$ catalyst (Fig. 1). The catalyst pre-reduced at 500 °C (designated $Co/Ba/La_2O_3$_500red) showed little NH_3 synthesis activity at 300 °C, but the activity increased with increasing reaction temperature until a moderate activity was obtained at 450 °C. Compared with $Co/Ba/La_2O_3$_500red, $Co/Ba/La_2O_3$_600red and $Co/Ba/La_2O_3$_700red both showed greater NH_3 synthesis activity across the whole reaction temperature range examined, and $Co/Ba/La_2O_3$_800red showed an activity between that of $Co/Ba/La_2O_3$_600red and $Co/Ba/La_2O_3$_700red. The apparent activation energy of the $Co/Ba/La_2O_3$ catalyst was found to decrease from 73.1 to 45.7 kJ mol^{-1} as the reduction temperature was increased from 500 to 700 °C (Fig. S1). Also, $Co/Ba/La_2O_3$_700red was found to have ammonia synthesis activity at reaction temperatures as low as 200 °C (synthesis rate, 0.3 mmol h^{-1} g^{-1}; Fig. S2).

Next, we examined the effect of adding Ba on the NH_3 synthesis rate of different Co and Ni catalysts (Fig. 2). At a reaction temperature of 350 °C, the NH_3 synthesis rate of $Co/Ba/La_2O_3$_700red was 19.3 mmol h^{-1} g^{-1}, which was 8.0 times that of $Co/Ba/La_2O_3$_500red and 6.9 times that of Co/La_2O_3_700red at the same temperature. Despite the activity's of $Co/Ba/La_2O_3$_700red being slightly lower than that of Co/Ba/MgO_700red, overall its activity was comparable with those reported for other Co catalysts, notwithstanding the different Co loadings, reaction pressures, and space velocities used in the previously reported studies (Table S1). For the Ni catalysts, reduction at high temperature and the addition of Ba were also found to have positive effects on NH_3 synthesis activity: the fact that the NH_3 synthesis rate of $Ni/Ba/La_2O_3$_700red was much higher than those of $Ni/Ba/La_2O_3$_500red and Ni/La_2O_3_700red at all temperatures suggested the possibility of activating Ni by using the same strategy used to activate Co.

We also examined the effect of reaction pressure on the NH_3 synthesis rate at 350 °C and compared the rates with $Co/Ba/La_2O_3$_700red to those with two benchmark Ru catalysts,

Cs^+/Ru/MgO and Ru/CeO_2 (Fig. 3). Cs^+/Ru/MgO is a well-known Ru catalyst with high NH_3 synthesis activity [41-44]. Ru/CeO_2 is a candidate catalyst for use in ammonia synthesis processes that use renewable energy [45]. At 0.1 MPa, the NH_3 synthesis rate of Co/Ba/La_2O_3_700red was lower than those of Cs^+/Ru/MgO_500red and Ru/CeO_2_500red. However, when the reaction pressure was increased, the NH_3 synthesis rate of Co/Ba/La_2O_3_700red increased drastically, whereas those of the two Ru catalysts increased only slightly. As a result, the NH_3 synthesis rate of Co/Ba/La_2O_3_700red at 1.0 MPa and at 3.0 MPa exceeded the rates of the two benchmark catalysts (synthesis rate at 3.0 MPa: Co/Ba/La_2O_3_700red, 35.7 mmol $h^{-1}g^{-1}$; Ru/CeO_2_500red, 13.7 mmol $h^{-1}g^{-1}$; and Cs^+/Ru/MgO_500red, 11.4 mmol $h^{-1}g^{-1}$). We also examined the NH_3 synthesis rate of Co/La_2O_3_700red and found that it was much lower than the rates of the other catalysts at all pressures.

To investigate the cause of the different pressure dependences, we performed a kinetic analysis at 350 °C and 0.1 MPa using the same four catalysts (Table 1 and Figs. S3 and S4). The fact that the reaction order with respect to N_2 was almost unity for all of the catalysts indicated that the rate-determining step was dissociation of molecular N_2. However, the fact that the reaction order with respect to H_2 was −0.18 and −0.76 for Ru/CeO_2_500red and Cs^+/Ru/MgO _500red, respectively, indicated that H atoms strongly adsorbed onto the Ru surface and inhibited activation of molecular N_2; this is referred to as hydrogen poisoning and is a typical drawback of Ru catalysts. In contrast, the positive reaction orders with respect to H_2, +0.43 and +0.32, that were obtained for Co/Ba/La_2O_3_700red and Co/La_2O_3_700red, respectively, indicated that these catalysts were free from hydrogen poisoning and that N_2 activation was promoted with increasing hydrogen pressure. A large negative reaction order with respect to NH_3 (−0.51) was obtained for Co/La_2O_3_700red, but this value was reduced to −0.17 with the addition of Ba. These findings suggest that it is difficult for the ammonia yield of Co/La_2O_3_700red to approach the equilibrium value because adsorbed NH, NH_2, and NH_3 inhibit the reaction. However, the addition of Ba can be expected to promote the desorption of such adsorbates and thus accelerate the reaction, even

near equilibrium. Together, these results indicate that Co catalysts may be a viable alternative to Ru catalysts.

3.2. Effects of doping with Ba

To understand more about the effects of Ba doping, we compared the physicochemical properties of Co/Ba/La_2O_3_700red and Co/La_2O_3_700red (Table 2). The specific surface areas of the two catalysts were comparable, but the mean Co particle size, as measured by STEM, was much smaller for Co/Ba/La_2O_3_700red than for Co/La_2O_3_700red (20 nm vs. 70 nm). The indication was that the addition of Ba inhibited sintering of the Co particles during reduction. Assuming the Co particles were cubic, this difference in particle size corresponds to 3.5-times greater Co dispersion for Co/Ba/La_2O_3_700red compared with Co dispersion for Co/La_2O_3_700red. On the other hand, the H_2 chemisorption value (a measure of the Co dispersion) of Co/Ba/La_2O_3_700red was found to be only 1.6-times greater than that of Co/La_2O_3_700red. The indication was that the surface of the Co particles in Co/Ba/La_2O_3_700red was partly covered by the support material. Also, the turnover frequency (TOF) of Co/Ba/La_2O_3_700red was about 4.4 times that of Co/La_2O_3_700red. Together, these results indicate that the drastic increase in NH_3 synthesis rate observed as a result of doping with Ba was the combined result of inhibition of Co particle sintering and an increase of TOF.

To understand how doping with Ba affected the state of the Co, we subjected Co/Ba/La_2O_3_700red and Co/La_2O_3_700red to XANES analysis. The fact that the Co K-edge XANES spectra of the two catalysts were comparable with that of Co foil indicated that the Co atoms in the catalysts were fully reduced to a metallic state after reduction at 700 °C.

Next, we investigated the morphology of Co/Ba/La_2O_3_700red by means of Cs-STEM and EELS. To avoid any unwanted structural or state changes, we used a special holder with a gas cell that allowed the sample to be transferred from the reactor to the STEM apparatus under an inert gas environment [35]. HADF-STEM images revealed that the Co particles were encapsulated by

a 2–3-mm-thick nano-fraction (Fig. 5a and Fig. S9). EELS mapping revealed that Ba and La elements were enriched in the nano-fraction(Figs. 5b, 5c, 4d, 5e). Although a low abundance of Ba was included overall in the catalyst (Ba:La molar ratio, 5:95), a high abundance of Ba was observed in the nano-fraction. In contrast, the fact that carbon element was not detected in the nano-fraction (Fig. 5f, 5g, 5h) indicated that the nano-fraction was an oxide or hydroxide of Ba or La.

3.3. Effect of reduction temperature

Finally, to understand the effects of reduction temperature on Co/Ba/La_2O, we investigated the physicochemical properties of the catalyst after reduction at different temperatures. With the increase in reduction temperature from 500 to 700 to 800 °C, the specific surface area decreased from 37.5 to 24.9 to 10.1 $m^2\ g^{-1}$, and the mean diameter of the Co particles increased from 10 to 20 to 34 nm. The indication was that greater sintering occurred at higher reduction temperature (Table 2). It must be noted that, the fact that the mean Co particle size was comparable both before and after exposure of Co/Ba/La_2O_3_700red to air indicated that exposure to air had no effect on Co particle size (see Figs. 5, S7, and S9). Also, the number of exposed Co particles decreased and the TOF drastically increased from 0.019 to 0.223 to 0.304 with increasing reduction temperature.

To understand why the TOF after reduction at 700 °C was more than 12 times the TOF after reduction at 500 °C, we characterized the catalysts by using several methods. To investigate the state of Co, we measured Co-K edge XANES spectra in as-prepared Co/Ba/La_2O_3 and Co/Ba/La_2O_3 pre-reduced at different temperatures (Fig. 4). The fact that the spectra for Co/Ba/La_2O_3_500red and Co/Ba/La_2O_3_700red were comparable with that for Co foil indicated that inactive oxidic Co was reduced to a metallic state after reduction at ≥500 °C.

To investigate the surface state of Co/Ba/La_2O_3_500red, we performed Cs-STEM and EELS observations without exposing the catalyst to the air (Figs. 6 and S10). In contrast to the findings for Co/Ba/La_2O_3_700red (Figs. 5 and S9), the Co particles in Co/Ba/La_2O_3_500red were not well

crystalized and were partially surrounded by a cloud-like substance containing Ba, La, and carbon elements. The fact that carbon element was observed in parts of the cloud in Co/Ba/La_2O_3_500red indicated the presence of non-crystalized carbonate species of Ba and/or La, because crystalized carbonate species was not observed by XRD analysis (Fig. 6, Fig. S11). Recall that such carbon element was not observed for Co/Ba/La_2O_3_700red by EELS measurement (Figure 5 and S9). Carbonate species are acidic and as such decrease the electron-donating ability of the support material. Therefore, we concluded that one of the causes for the high TOF of Co/Ba/La_2O_3_700red was complete removal of La and Ba carbonate species during reduction at high temperature. It is likely that hydroxide species are also removed from the catalyst because the temperature-programmed reduction profile of fresh Co/Ba/La_2O_3 indicated that the formation of CH_4, CO, CO_2, and H_2O was completed at a temperature below 700 °C (Fig. 7). Thus, these data indicated that the low crystalline nano-fraction encapsulating the Co nanoparticles in Co/Ba/La_2O_3_700red was composed of BaO and La_2O_3. Therefore, another of the causes of the high TOF of Co/Ba/La_2O_3_700red was ascribed to encapsulation of the Co particles by the low crystalline nano-fraction of BaO-La_2O_3. Previously, based on density functional theory calculations and Fourier-transform infrared spectroscopy measurements after adsorption of molecular N_2 on the catalyst, we reported the high activity of Co nanoparticles encapsulated by BaO loaded on MgO (Co@BaO/MgO), which we ascribed to strong electron donation from BaO to N_2 via Co [35]. Although in the present study we were unable to fabricate a self-supporting disk of the Co/Ba/La_2O_3 catalyst that transmitted infrared light and therefore could not use Fourier-transform infrared spectroscopy, the high TOF of Co/Ba/La_2O_3_700red may also be due to such electron donation from BaO-La_2O_3 to the antibonding π-orbital of the N≡N bond of molecular N_2. We also found that increasing the reduction temperature up to 800 °C further increased the TOF; however, the NH_3 synthesis rate decreased due to sintering of the Co particles (Table 2).

Co/Ba/La_2O_3_700red and Co/Ba/MgO_700red showed comparable TOFs, but the NH_3 synthesis rate (350 °C, 1 MPa) of Co/Ba/MgO_700red was 1.3 times that of Co/Ba/La_2O_3_700red.

These results indicated that fundamentally the core (Co) - shell ($BaO\text{-}La_2O_3$) structure enhanced the NH_3 synthesis ability of surface Co, and that the difference of NH_3 synthesis rate between these catalysts was due to the difference of the mean Co particle size (i.e., 10.6 vs. 20 nm for Co/Ba/MgO_700red and $Co/Ba/La_2O_3$_700red). The higher surface area of Co/Ba/MgO_700red (47.6 $m^2\ g^{-1}$) compared with that of $Co/Ba/La_2O_3$_700red likely contributed to the formation of fine Co nanoparticles. Thus, use of a basic support with a higher specific surface area is expected to afford catalysts with enhanced NH_3 synthesis rates.

3.4. Conclusions

Here, we demonstrated that encapsulation Co nanoparticles by $BaO\text{-}La_2O_3$ on La_2O_3 support exhibited high NH_3 synthesis activity under mild reaction conditions. The $Co/Ba/La_2O_3$ pre-reduced at 700 °C showed high NH_3 synthesis activity with a synthesis rate of 19.3 mmol $h^{-1}g^{-1}$ at 350 °C, which was 6.9 times that of nondoped parent catalyst. Moreover, the $Co/Ba/La_2O_3$ pre-reduced at 700 °C was active at temperatures down to 200 °C. We also found that addition of Ba to the catalyst inhibited sintering of the Co particles during reduction. Increasing the reduction temperature from 500 to 700 °C resulted in a drastic increase in TOF from 0.019 to 0.223. The increase in TOF was ascribed to encapsulation of Co particles by a $BaO\text{-}La_2O_3$ nano-fraction during high-temperature reduction. It is likely that donation of electrons from the nano-fraction to molecular N_2 via Co markedly promoted NH_3 synthesis. Furthermore, the elimination of ammonia poisoning by addition of Ba is a potential merit for carrying out the reaction near equilibrium. The present findings also indicate that these strategies are also likely appliable to Ni catalysts. Together, the present results provide information that will be useful for the development of highly active NH_3 synthesis catalysts for use in processes that use renewable energy.

Funding information

This work was supported by the Japan Science and Technology Agency [grant number JPMJCR1341]; the TOYOTA Mobility Foundation; the Japan Society for the Promotion of Science [grant number 20H02522]; and the Ministry of Education, Culture, Sports, Science and Technology of Japan [grant numbers JPMXP09-A-19-KU-0332, JPMXP09-A-20-KU-0344, MXP0112101003]. X-ray absorption measurements were performed at the BL01B1 beamline of Spring-8 at the Japan Synchrotron Radiation Research Institute (No. 2018B1345).

Author contributions

K.N. designed the project. K.S. coordinated all the characterization work and contributed to the data analysis for this project. S-I.M., Y.O., K.T., K.I., and Y.W. prepared the catalysts, performed the characterizations, and tested catalytic activities. K.S. conducted X-ray absorption fine structure measurement. T.T., T.Y., and S.M. conducted the Cs-STEM observations and energy electron loss spectroscopy analysis. S-I.M., K.S., and K.N. co-wrote the manuscript.

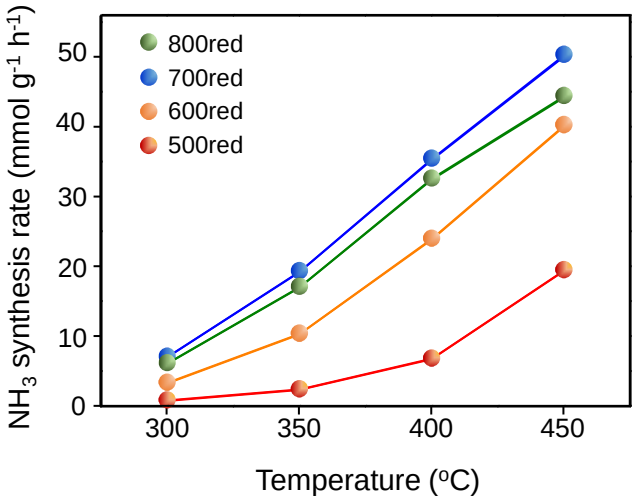

Figure 1. Influence of reduction temperature on NH_3 synthesis rate of $Co/Ba/La_2O_3$ at 1.0 MPa.

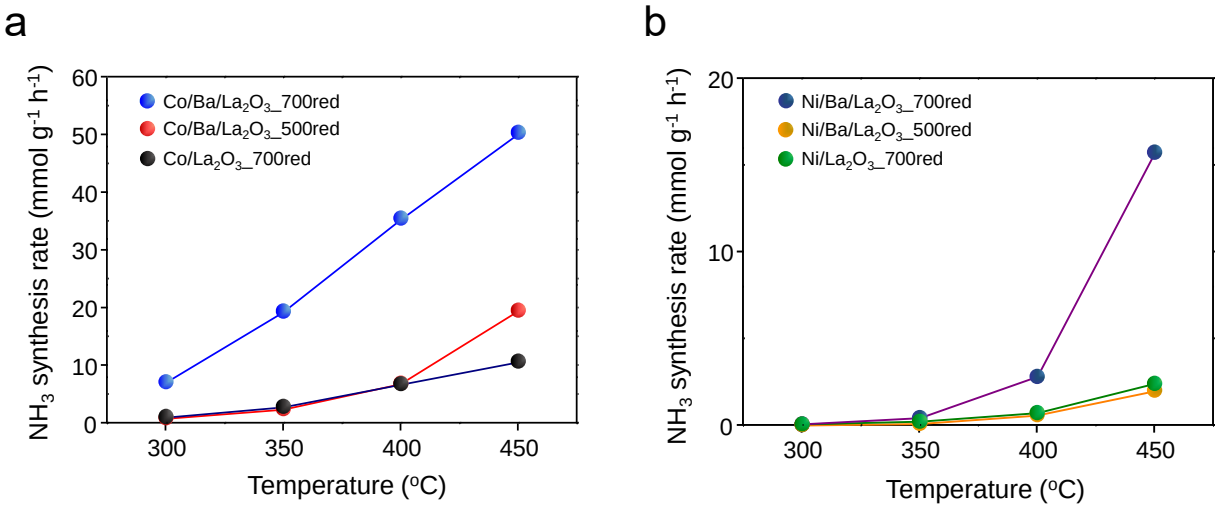

Figure 2. Temperature dependence of the NH_3 synthesis activities of supported Co and Ni catalysts at 1.0 MPa. The catalysts were pre-reduced at 500 ºC and 700 ºC (xxxred means the catalyst was pre-reduced at xxx). (a) Supported Co catalysts. (b) Supported Ni catalysts.

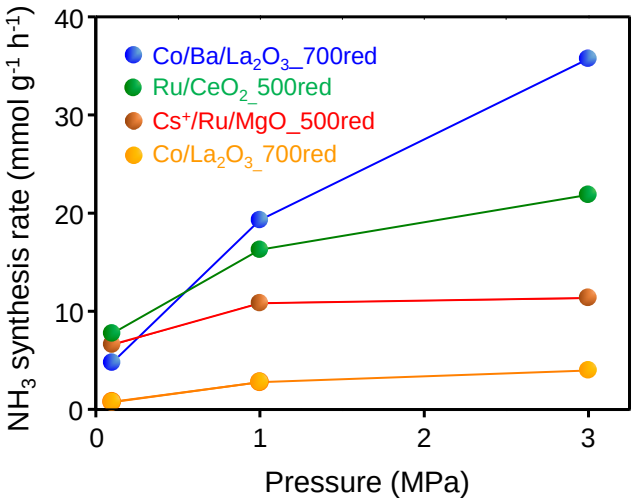

Figure 3. Pressure dependence of the NH_3 synthesis activities of $Co/Ba/La_2O_3$_700red, Co/La_2O_3_700red, and two benchmark Ru catalysts at 350 °C.

Table 1. Results of a kinetic analysis over $Cs^+/Ru/MgO$, Ru/CeO_2, $Co/Ba/La_2O_3$, or Co/La_2O_3.

Catalyst	Order[a]		
	n[a]	h[b]	a[c]
$Cs^+/Ru/MgO$_500red	1.07	−0.76	−0.15
Ru/CeO_2_500red	0.85	−0.18	−0.19
$Co/Ba/La_2O_3$_700red	0.85	0.43	−0.17
Co/La_2O_3_700red	0.97	0.32	–0.51

[a] Reaction order with respect to N_2. [b] Reaction order with respect to H_2. [c] Reaction order with respect to NH_3.

Table 2. Physicochemical properties and catalytic performances of supported co catalysts.

Catalyst	SSA[a] [$m^2\ g_{cat}^{-1}$]	H_2 chemisorption[b] [$\mu mol\ g^{-1}$]	d[c] [nm]	Rate[d] [$mmol\ g_{cat}^{-1}\ h^{-1}$]	TOF[e] [s^{-1}]
Co/Ba/La_2O_3_500red	37.5	35.0	10	2.4	0.019
Co/Ba/La_2O_3_700red	24.9	24.1	20	19.3	0.223
Co/Ba/La_2O_3_800red	10.1	15.6	34	17.1	0.304
Co/La_2O_3_700red	25.8	14.9	70	2.8	0.051

[a] Specific surface area.

[b] Measured using H_2 chemisorption capacity.

[c] Mean particle size of Co nanoparticles, as estimated by Cs-STEM (see Figs. S5–8).

[d] At 350 ºC and 1.0 MPa.

[e] Turnover frequency. Calculated from the H_2 chemisorption value and the NH_3 synthesis rate (see Table 1).

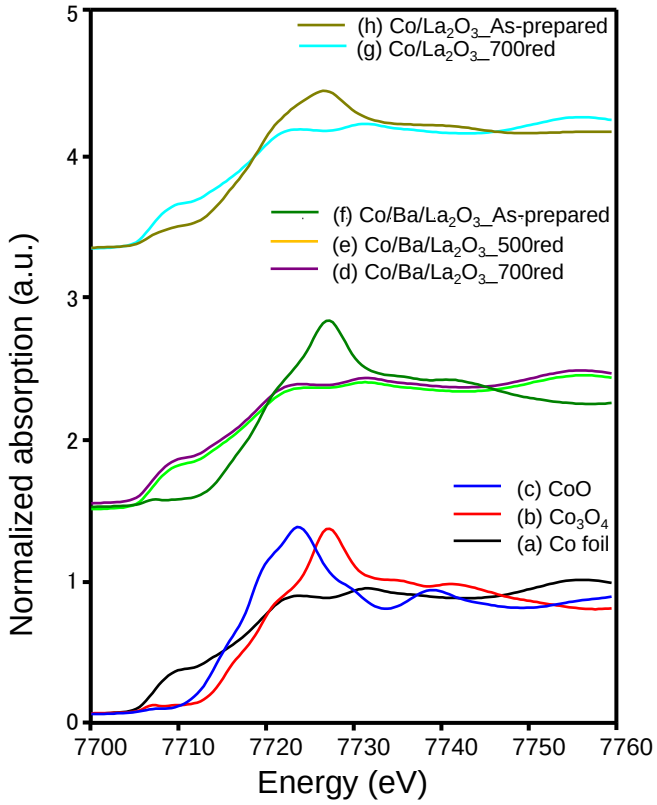

Figure 4. Normalized Co K-edge XANES spectra for Co/La_2O_3 and $Co/Ba/La_2O_3$ catalysts pre-reduced at different temperatures, and for several reference samples.

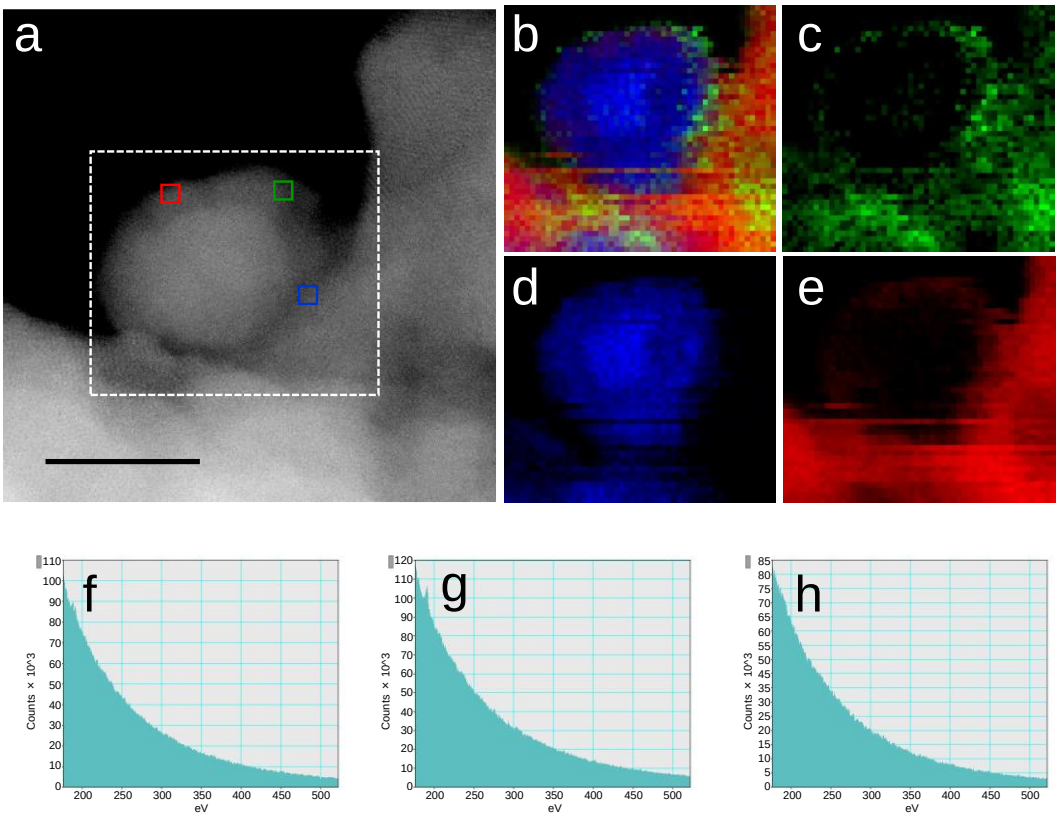

Figure 5. High-angle annular dark-field scanning transmission electron microscopy image and energy-dispersive X-ray maps of Co/Ba/La_2O_3_700red without exposure to air. (a) High-angle annular dark-field image of the catalyst. (b–e) Energy-dispersive X-ray maps of (b) overlay, (c) Ba L, (d) Co L, (e) La L in the area within the white, dotted square in (a). (f–h) C K energy electron loss spectroscopy spectra of the areas indicated by the green (f), blue (g), and red (h) squares in (a).

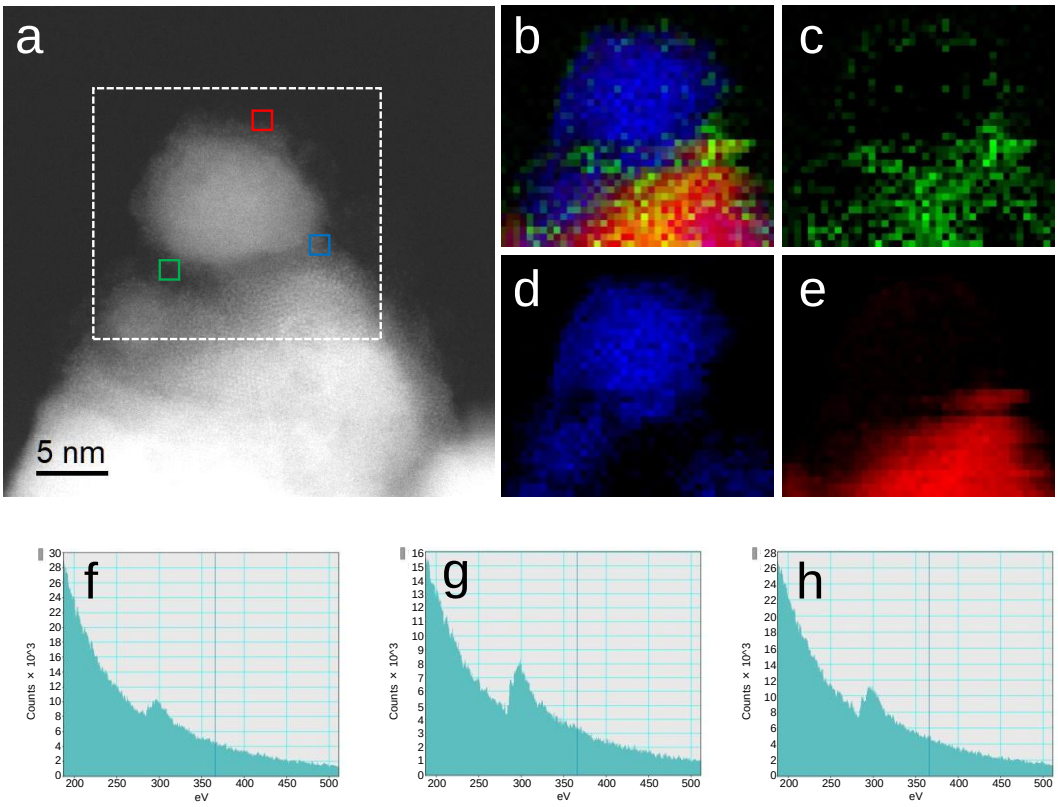

Figure 6. High-angle annular dark-field scanning transmission electron microscopy image and energy-dispersive X-ray maps of Co/Ba/La_2O_3_500red without exposure to air. (a) High-angle annular dark-field image of the catalyst. (b–e) Energy-dispersive X-ray maps of (b) overlay, (c) Ba L, (d) Co L, (e) La L in the area within the white, dotted square in (a). (f–h) C K energy electron loss spectroscopy spectra of the areas indicated by the green (f), blue (g), and red (h) squares in (a).

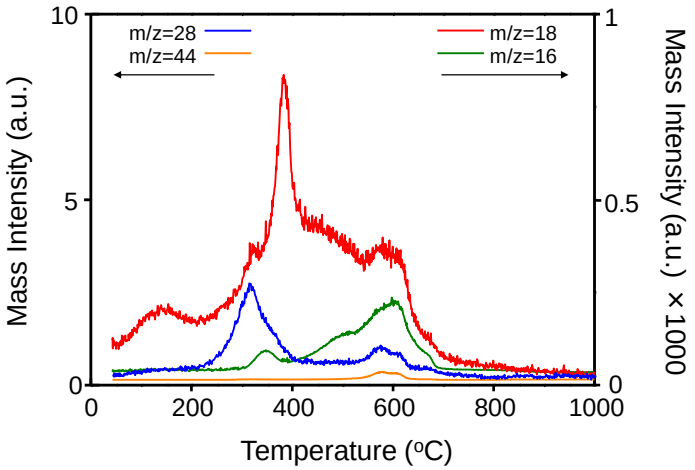

Figure 7. H_2-temperature-programmed reduction profiles for as-prepared $Co/Ba/La_2O_3$ catalyst.

References

[1] J. W. Erisman, M. A. Sutton, J. Galloway, Z. Klimont, W. Winiwarter, Nature Geoscience, How a century of ammonia synthesis changed the world 1 (2008) 636–639.

[2] V. Smil, Detonator of the population explosion, Nature 400 (1999) 415.

[3] J. Galloway, A. Towmsent, J. W. Erisman, M. Dekumda, Z. Cai, J. Frendy, L. Maryinelli, Transformation of the Nitrogen Cycle: Recent Trends, Questions, and Potential Solutions, Science 320 (2008) 889-892.

[4] T. Kandemir, M. Schuster, A. Senyshyn, M. Bebrens, R. Schlogl, The Haber-Bosch Process Revisited: On the Real Structure and Stability of "Ammonia Iron" under Working Conditions, Angewandte Chemie International Edition 52 (2013) 12723-12726.

[5] R. Schlogl, Catalystic Synthesis of Ammonia-A"Never Ending Story"?, Angewandte Chemie International Edition 42 (2003) 2004-2008.

[6] R. F. Service, Liquid sunshine, Science 361 (6398) (2018) 120-123.

[7] C. Smith, A. K. Hill, L. T. Murciano, Current and future role of Haber-Bosch ammonia in a carbon-free energy landscape, Energy & Environmental Science 13 (2020) 331-334.

[8] I. Rafiqul, C. Weber, B. Lehmann, A. Voss, Energy efficiency improvements in ammonia production – perspectives and uncertainties, Energy 30 (13) (2005) 2487-2504.

[9] D. Miura, T. Tezuka, A comparable study of ammonia energy systems as a future energy carrier, with particular reference to vehicle use in Japan 68 (2014) 428-436.

[10] A. J. Pool, E. Lobkovsky and P. J. Chirik, Hydrogenation and cleavage of dinitrogen to ammonia with a zirconium complex, Nature 427 (2004) 527-530.

[11] S. Foster, S. I. P. Bakovic, R. D. Duda, S. Maheshwari, R. D. Milton, S. H. Minteer, M. J. Janik, J. N. Renner, L. F. Greenlee, Catalysts for nitrogen reduction to ammonia, Nature Catalysts 1 (2018) 490-500.

[12] H. K. Chae, D. Y. Siberio-Perez, J. Kim, Y. Go, M. Eddaoudi, A. J. Matzger, M. O'Keeffe, M. Yaghi, A route to high surface area, porosity and inclusion of large molecules in crystals,

Nature 427 (2004) 523-527.

[13] S. Gambarotta, J. Scott, Multimetallic Cooperative Activation of N_2, Angewandte Chemie International Edition 43 (2004) 5298-5308.

[14] K. Sato, S. Miyahara, Y. Ogura, K. Tsujimaru, Y. Wada, T. Toriyama, T. Yamamoto, S. Matsumura, K. Nagaoka, Surface Dynamics for Creating Highly Active Ru Sites for Ammonia Synthesis: Accumulation of a Low-Crystalline, Oxygen -Deficient Nanofraction, ACS Sustainable Chemistry & Engineering 8 (7) (2020) 2726-2734.

[15] A. K. Hill, L. Torrente-Murciano, Low temperature H_2 production from ammonia using ruthenium-based catalysis Synergetic effect of promoter and support, Applied Catalysts B: Environment 172-173 (2015) 129-135.

[16] Y. Ogura, K. Sato, S. Miyahara, Y. Yukiko, T. Yamamoto, S. Matsumura, K. Nagaoka, Efficient ammonia synthesis over a $Ru/La_{0.5}Ce_{0.5}O_{1.75}$ catalyst pre-reduced at high temperature, Chemical Science 9 (2018) 2230-2237.

[17] M. Kitano, Y. Inoue, Y. Yamazaki, F. Hayashi, S. Kanbara, S. Matsushi, T. Yokoyama, S. W. Kim, M. Hara, H. Hosono, Ammonia synthesis using a stable electride as an electron donor and reversible hydrogen store, Nature Chemical 4 (2012) 934-940.

[18] K. Sato, K. Nagaoka, Boosting Ammonia synthesis under Mild Reaction Conditions by Precise Control of the Basic Oxide-Ru Interface, Chemical Letter 10 (2020) 1246.

[19] Y. Kobayashi, Y. Tang, H. Yamashita, N. Masuda, S. Hosokawa, H. Kageyama, Titanium-Based Hydrides as Heterogeneous Catalysts for Ammonia Synthesis, Journal of the American Chemical Society 139 (2017) 18240-18246.

[20] M. Kitano, Y. Inoue, M. Sasase, K. Kishida, Y. Kobayashi, K. Nishiyama, T. Tada, S. Kawamura, T. Yokoyama, M. Hara, H. Hosono, Self-organized Ruthenium-Barium Core-Shell Nanoparticles on a Mesoporous Calcium Amide Matrix for Efficient Low-Temperature Ammonia Synthesis, Angewandte Chemie International Edition 57 (2018) 2648-2652.

[21] M. Hattori, S. Iijima, T. Nakao, H. Hosono, M. Hara, Solid solution foracatalytic ammonia

synthesis from nitrogen and hydrogen gases at 50 °C, Nature Communication 11 (2020) 1-8.

[22] S. J. Wang, S. F. Yin, B. Q. Xu, C. F. Ng, C. T. Au, Investigation on modification of Ru/CNTs catalyst for the generation of Cox-free hydrogen from ammonia, Applied Catalysis B: Environmental 52 (2004) 287-299.

[23] L. Li, T. Zhang, J. Cai, H. Cai, J. Ni, B. Lin, J. Lin, X. Wang, L. Zheng, C. Au, L. Jiang, Operando spectroscopic and isotopic- label-directed observation of LaN-promoted Ru/ZrH_2 catalyst for ammonia synthesis via associative and chemical looping route, Journal of Catalysis 389 (2020) 218-228.

[24] S. Y. Chen, M. Nishi, A. Chang, W. C. Hsiao, T. Mochizuki, H. Takagi, C. M. Yang, Well-ordered Cs-Ru/@SBA-15 nanocomposite materials for low pressure ammonia synthesis 4 (2020) 5802-5811.

[25] J. Z. Qiu, J. Hu, J. Lan L. F. Wang, G. Fu, R. Xiao, B. Ge, J. Jiang, Pure Siliceous Zeolite-Supported Ru Single-Atom Active Sites for Ammonia Synthesis, Chemistry of Materials 31 (2019) 9413-9421.

[26] Y. Ma, G. Lan, X. Wang, G. Zhang, W. Han, H. Tang, H. Liu, Y. Li, Effect of nitrogen Co-doping with ruthenium on the catalysts for ammonia synthesis 9 (2019) 22045-22052.

[27] X. Wang, X. Peng, H. Ran, B. Lin, J. Ni, J. Lin, L. Jiang, Influence of Ru Substitution on the Properties of $LaCoO_3$ Catalysts for Ammonia synthesis: XAFS and XPS Studies, Industrial & Engineering Chemistry Research 57 (2018) 17375-17383.

[28] K. Narasimharao, P. Seetharamulu, K. S. R. Rao, S. N. Basahel, Carbon covered Mg-Al hydrotalcite supported nanosized Ru catalysts for ammonia synthesis, Journal of Molecular Catalysis A: Chemical 411 (2016) 157-166.

[29] L. Zhang, J. Lin, J. Ni, R. Wang, K. Wei, Highly efficient Ru/Sm_2O_3-CeO_2 catalyst for ammonia synthesis, Catalysis Communications 15 (2011) 23-26.

[30] J. Huang, M. Yuan, X. Li, Y. Wang, M. Li, J. Li, J. Z. You, Inhibited hydrogen poisoning for enhanced activity of promoters-Ru/$Sr_2Ta_2O_7$ nanowires for ammonia synthesis 389 (2020)

556-565.

[31] B. Lin, Y. Liu, L. Heng, J. Ni, J. Lin, L. Jiang, Effect of ceria morphology on the catalytic activity of Co/CeO_2 catalyst for ammonia synthesis, Catalysis Communications 101 (2017) 15-19.

[32] S. Hargen, R. Barfod, R. Fehrmann, C. J. H. Jacobson, H. T. Teunissen, I. Chorkendorff, Ammonia synthesis with barium-promoted iron-coblt alloys supported carbon, Journal of Catalysis 214 (2003) 327-335.

[33] B. Lin, Y. Qi, K. Wei, J. Lin, Effect of pretreatment on ceria-supported cobalt catalyst for ammonia synthesis, RSC Advance 4 (2014) 38093-38102.

[34] A. Vojvodic, A. J. Medford, F. Studt, F. A. Pedersen, T. S. Khan, T. Bligaard, J. K. Norskov, Exploring the limits; A low pressure, low temperature Haber-Bosh-process., Chemical Physics Letter 598 (2014) 108-112.

[35] K. Sato, S. Miyahara, K. Tsujimaru, Y. Wada, T. Toriyama, T. Yamamoto, S. Matsumura, K. Inazu, H. Mori, T. Iwasa, T. Taketsugu, K. Nagaoka, Barium Oxide Encapsulating Cobalt Nanoparticles Supported on Magnesium Oxide: Active Non-noble Metal Catalyst for Ammonia Synthesis under Mild Reaction Conditions 11 (2021) 13050-13061.

[36] S. Miyahara, K. Sato, Y. Kawano, K. Imamura, Y. Ogura, K. Tsujimaru, K. Nagaoka, Ammonia synthesis over lanthanoid oxide-supported ruthenium catalysts, Catalysts Today 376 (2021) 36-40.

[37] K. Sato, K. Imamura, Y. Kawano, S. Miyahara, T. Yamamoto, S. Matsumura, K. Nagaoka, A low-crystalline ruthenium nano-layer supported on praseodymium oxides as an active catalyst for ammonia synthesis, Chemical Science 8 (1) (2017) 674-679.

[38] Y. Ogura, K. Tsujimaru, K. Sato, S. Miyahara, T. Toriyama, T. Yamamoto, S. Matsumura, K. Nagaoka, A $Ru/La_{0.5}Pr_{0.5}O_{1.75}$ catalyst low-temperature ammonia synthesis, ACS Sustainable Chemistry & Engineering 6 (2018) 17258–17266.

[39] R. Kojima, K. Aika, Cobalt molybdenum bimetallic nitride catalysts for ammonia synthesis:

Part 2. Kinetic study, Applied Catalysis A: General 218 (1-2) (2001) 121-128.

[40] K. Imamura, S. Miyahara, Y. Kawano, K. Sato, Y. Nakasaka, K. Nagaoka, Kinetics of ammonia synthesis over Ru/Pr_2O_3, Journal of the Taiwan Institute of Chemical Engineers 105 (2019) 50-56.

[41] R. Kojima, K. Aika, Cobalt molybdenum bimetallic catalysts for ammonia synthesis. Part 2. Kinetic study, Applied Catalysis A: General 218 (2001) 121-128.

[42] K. Aika, Role of alkali promoter in ammonia synthesiw over ruthenium catalysts-Effect on reaction mechanism, Catalysis Today 286 (2017) 14.

[43] R. Javaid, H. Matsumoto, T. Nanba, Influence of reaction conditions and promoting role of ammonia produced at higher temperature conditions in its synthesis process over Cs-Ru/MgO catalyst, Chemistry 4 (2019) 2218-2224.

[44] S. E. Siporin, R. J. Davis, Use of kinetic models to explore the role of base promoters on Ru/MgO ammonia synthesis catalysts, Journal of Catalysis 225 (2) (2004) 359-368.

[45] T. Nanba, Y. Nagata, K. Kobayashi, R. Javaid, R. Atsumi, M. Nishi, T. Mochizuki, Y. Manaka, H. Kojima, T. Tsujimura, H. Matsymoto, T. Fujimoto, K. Suzuka, T. Oouchi, S. Kameda, Y. Hoshino, S. Fujimoto, M. Kai, Y. Fujimura, Explorative Study of Ru/CeO_2 Catalyst for NH_3 Synthesis from Renewable Hydrogen and Demonstration of NH_3 Synthesis under a Range of Reaction Condition, Journal of the Japan Petroleum Institute 64 (1) (2021) 1-9.

Supplementary Material

Co/Ba/La_2O_3 catalyst for ammonia synthesis under mild reaction conditions

Shin-ichiro Miyahara,[a] Katsutoshi Sato,*[a,b] Yuta Ogura,[a] Kotoko Tsujimaru,[c] Yuichiro Wada,[c] Takaaki Toriyama,[d] Tomokazu Yamamoto,[e] Syo Matsumura,[d,e] Koji Inazu,[f] and Katsutoshi Nagaoka*[a]

---

[a] Department of Chemical Systems Engineering, Graduate school of Engineering, Nagoya University, Furo-cho, Chikusa-ku, Nagoya, 464-8603, Japan

[b] Elements Strategy Initiative for Catalysts and Batteries, Kyoto University, 1-30 Goryo-Ohara, Nishikyo-ku, Kyoto, 615-8245, Japan

[c] Department of Integrated Science and Technology, Faculty of Science and Engineering, Oita University, 700 Dannoharu, Oita, 870–1192, Japan

[d] The Ultramicroscopy Research Center, Kyushu University, Motooka 744, Nishi-ku, Fukuoka, 819- 0395, Japan

[e] Department of Applied Quantum Physics and Nuclear Engineering, Kyushu University, Motooka 744, Nishi-ku, Fukuoka, 819-0395, Japan

[f] National Institute of Technology, Numazu College, 3600 Ooka, Numazu, Shizuoka, 410-8501, Japan

***Corresponding authors**

K. Sato: sato.katsutoshi@marerial.nagoya-u.ac.jp

K. Nagaoka: nagaoka.katsutoshi@material.nagoya-u.ac.jp

Additional details for the Experimental section

Kinetic analysis

Reaction kinetics were analyzed as previously reported [1,2]. Reaction orders with respect to N_2, H_2, and NH_3 were determined by measuring N_2, H_2, and NH_3 pressure dependence for the ammonia synthesis rates on the assumption that the rate (r) was described by expression (1). Equations (2) to (5) were also used for this analysis:

$$r = kP_{N_2}^{n} P_{H_2}^{h} P_{NH_3}^{a} \quad (1)$$

$$r = \frac{(1/w)dy_o}{d(1/q)} \quad (2)$$

$$\log y_o = \log \left(\frac{C}{q} \right)^{\frac{1}{m}} \quad (3)$$

$$r = \left(\frac{1}{w} \right) \left(\frac{C}{m} \right) y_o^{(1-m)} \quad (4)$$

$$C = k_2 P_{H_2}^{h} P_{N_2}^{n} \quad (5)$$

where r, w, y_0, q, C, and $(1 - m)$ denotes the ammonia synthesis rate, catalyst mass, ammonia mole fraction at the reactor outlet, flow rate, a constant, and a, respectively. Kinetic analyses were performed at 350 °C and 0.1 MPa. Other reaction conditions are described in Table S2. To avoid any contribution from the reverse reaction, kinetic measurements were carried out at a space

velocity where the ammonia concentration at the reactor exit was far from the thermodynamic equilibrium concentration.

Supplementary results

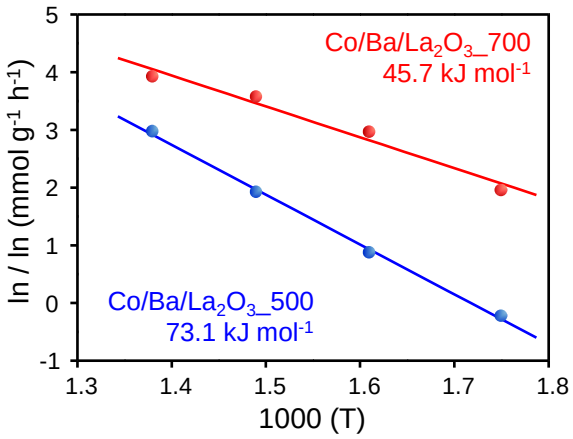

Figure S1. Arrhenius plots for the ammonia synthesis reaction at 1.0 MPa.

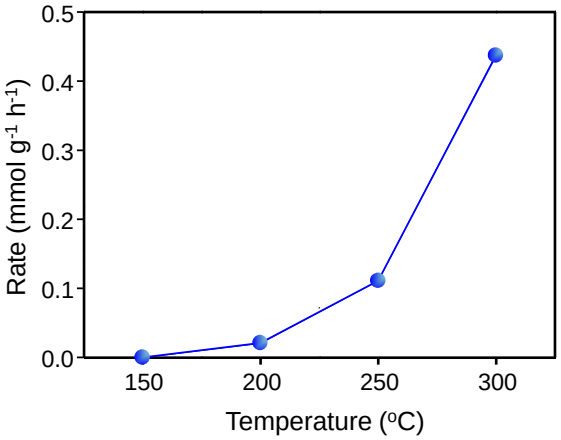

Figure S2. Influence of reaction temperature on the ammonia synthesis rate of $Co/Ba/La_2O_3$_700red at low temperatures.

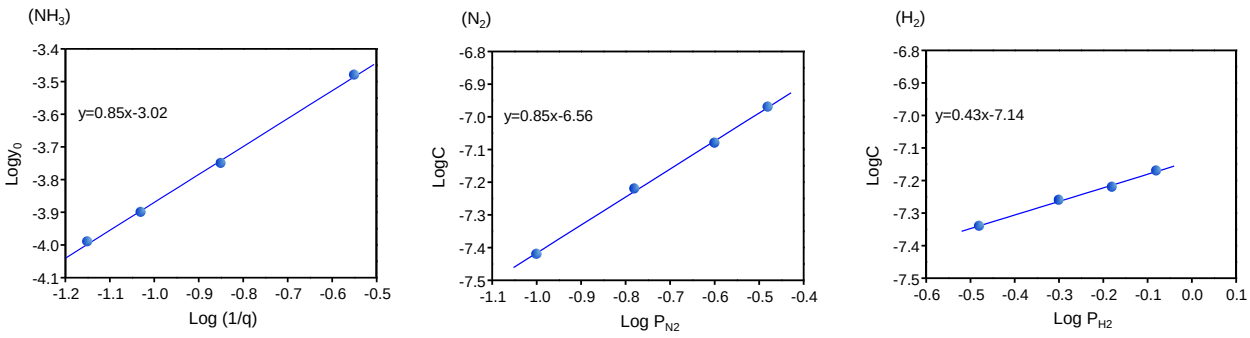

Figure S3. Graphs for estimating reaction orders over Co/Ba/La_2O_3_700 at 350 °C and 0.1 MPa.

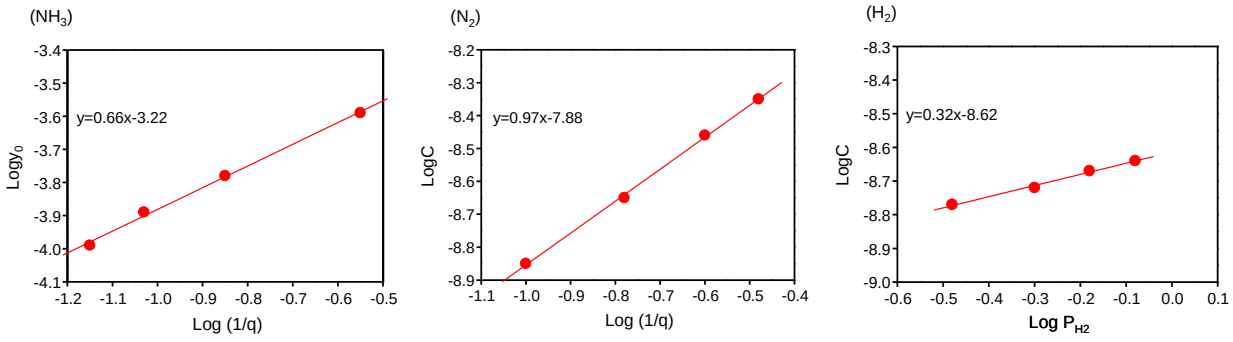

Figure S4. Graphs for estimating reaction orders over Co/La_2O_3_700 at 350 °C and 0.1 MPa.

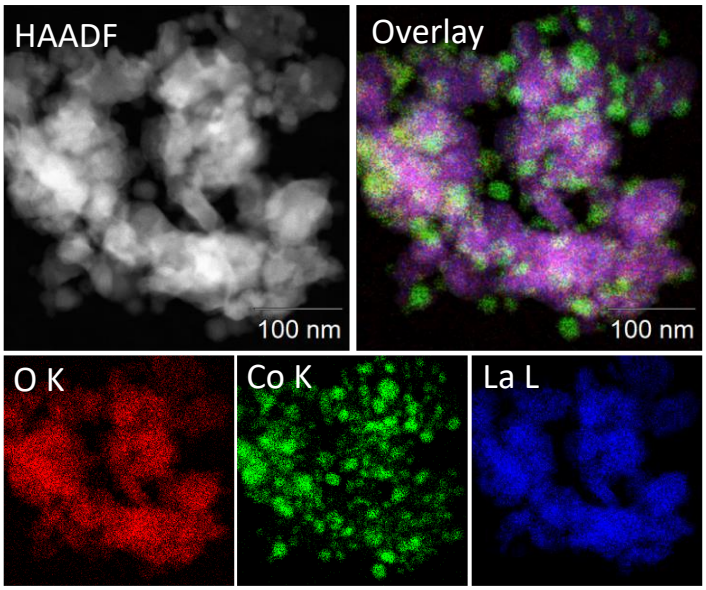

Figure S5. High-angle, annular, dark-field scanning transmission electron microscopy image and energy-dispersive X-ray maps of Co/Ba/La_2O_3 catalyst after reduction at 700 °C. The energy-dispersive X-ray map for Ba could not be used because the small peak attributed to Ba overlapped the large peak attributed to La.

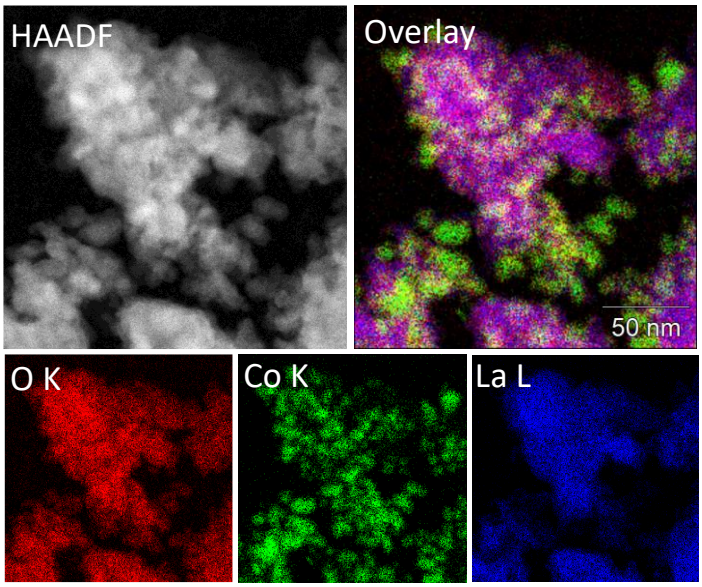

Figure S6. High-angle annular dark-field scanning transmission electron microscopy image and energy-dispersive X-ray maps of Co/Ba/La_2O_3 catalyst after reduction at 500 °C. The energy-dispersive X-ray map for Ba could not be used because the small peak attributed to Ba overlapped the large peak attributed to La.

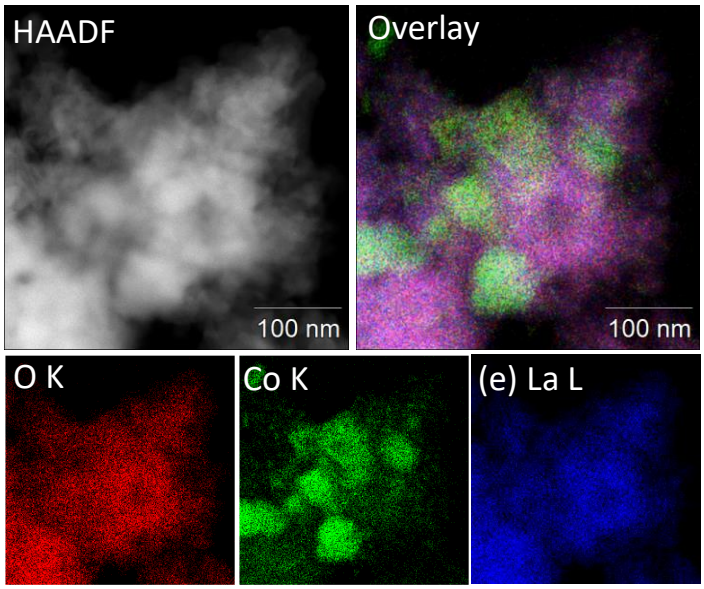

Figure S7. High-angle annular dark-field scanning transmission electron microscopy image and energy-dispersive X-ray maps of Co/La_2O_3 catalyst after reduction at 700 °C. The energy-dispersive X-ray map for Ba could not be used because the small peak attributed to Ba overlapped the large peak attributed to La.

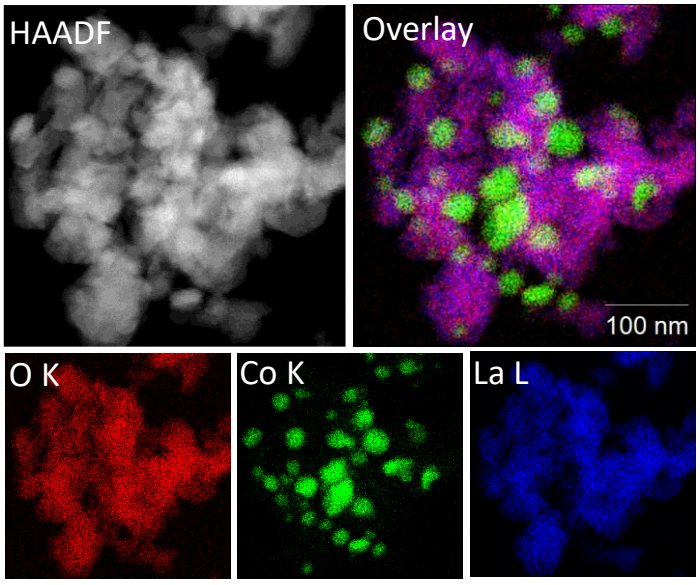

Figure S8. High-angle annular dark-field scanning transmission electron microscopy image and energy-dispersive X-ray maps of $Co/Ba/La_2O_3$ catalyst after reduction at 800 °C. The energy-dispersive X-ray map for Ba could not be used because the small peak attributed to Ba overlapped the large peak attributed to La.

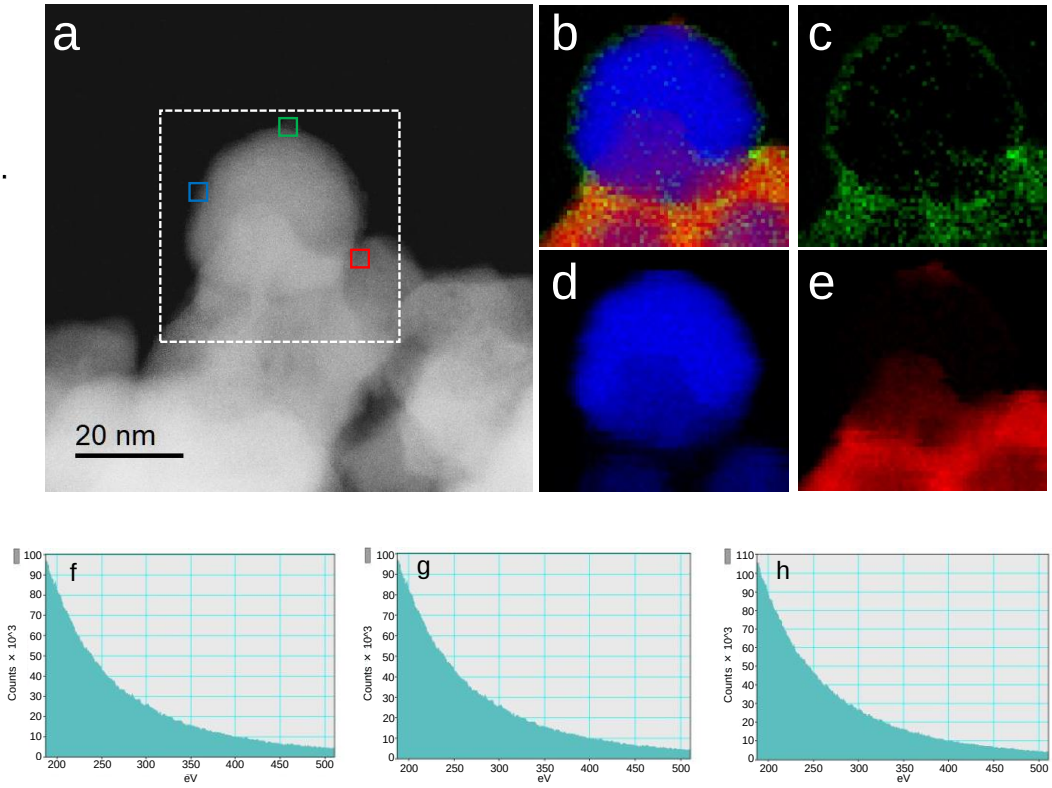

Figure S9. High-angle annular dark-field scanning transmission electron microscopy image and energy-dispersive X-ray maps of Co/Ba/La_2O_3_700red without exposure to air. (a) High-angle annular dark-field image of the catalyst. (b–e) Energy-dispersive X-ray maps of (b) overlay, (c) Ba L, (d) Co L, (e) La L in the area within the white, dotted square in (a). (f–h) C K energy electron loss spectroscopy spectra of the areas indicated by the green (f), blue (g), and red (h) squares in (a).

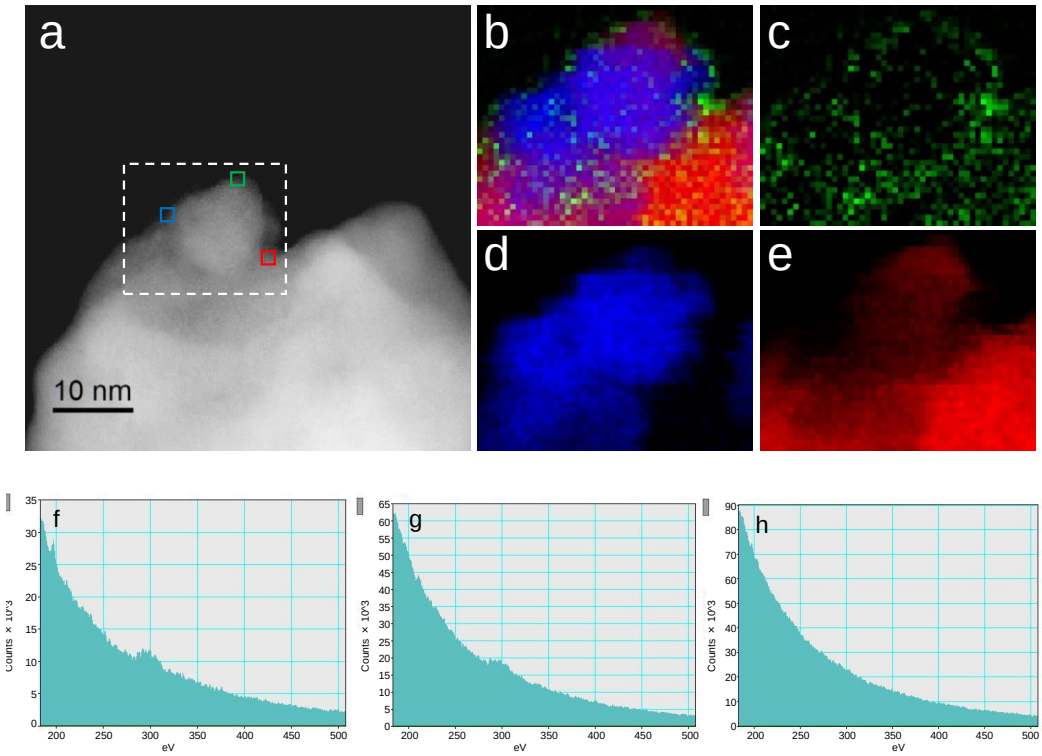

Figure S10. High-angle annular dark-field scanning transmission electron microscopy image and energy-dispersive X-ray maps of Co/Ba/La_2O_3_500red without exposure to air. (a) High-angle annular dark-field image of the catalyst. (b–e) Energy-dispersive X-ray maps of (b) overlay, (c) Ba L, (d) Co L, (e) La L in the area within the white, dotted square in (a). (f–h) C K energy electron loss spectroscopy spectra of the areas indicated by the green (f), blue (g), and red (h) squares in (a).

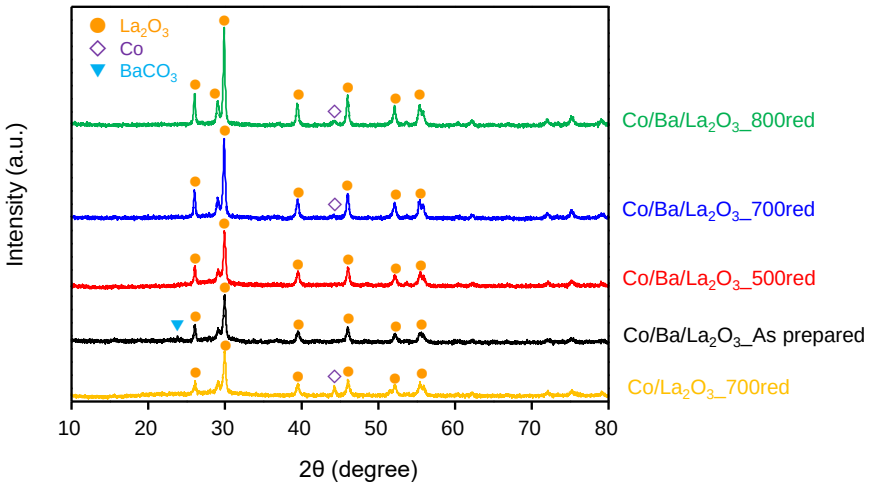

Figure S11. X-ray diffraction patterns for $Co/Ba/La_2O_3$ and Co/La_2O_3 after reduction at different temperatures.

Table S1. Activities of previously reported ammonia synthesis catalysts.

Catalyst	Co loading	Temperature	Pressure	Space velocity	Ammonia ratio	Reference
	wt%	ºC		mL h^{-1} g_{cat}^{-1}	mmol h^{-1} g_{cat}^{-1}	
Co/Ba/La_2O_3 700red	20	300	1 MPa	72,000	7.0	This work
	20	350	1 MPa	72,000	19.3	
	20	400	1.0 MPa	72000	35.4	
Co/Ba/MgO 700red	20	300	1 MPa	72,000	10.5	[3]
	20	350	1 MPa	72,000	24.6	
	20	400	1 MPa	72,000	43.9g	
Ba0.35-Co/C		400	10 bar	53,400	22.32	[4]
Co/Ba-Ca(NH2)2	8	300	0.9 MPa	36,000	6.6	[5]
	8	400	0.9 MPa	36,000	26	
Co/BaCeO3-xNyHz	4.7	400	0.9 MPa	36,000	10.1	[6]
	4.7	300	0.9 MPa	36,000	2.4	
Co/C12A7:e-	0	400	9 bar	18,000	3.8	[7]
BaH2-Co/CNTs	5.2	300	10 bar	60,000	4.8	[8]
3BaH2-Co/CNTs	10	400	10 bar	60,000	22	
BaO-Co/CNT	3.25	300	10 bar	60,000	0.03	
Co-C-N	3.73	350	1 MPa	36,000	4.3	[9]
LaCoSi	0	400	9 bar	36,000	5	[10]
Cs/Co3Mo3N	0	400	11 bar	9,000	5	[11]
Co-LiH	59.8	350	1 MPa	60,000	12	[12]
	0	300	10 bar	60,000	4.7	
CoBaTiO2.37H0.63	0.31	400	10 bar	66,000	3	[13]

References (SI)

[1] R. Kojima, K. Aika, Cobalt molybdenum bimetallic nitride catalysts for ammonia synthesis: Part 2. Kinetic study, Applied Catalysis A: General, 218 (1-2) (2001), pp. 121-128.

[2] K. Imamura, S. Miyahara, Y. Kawano, K. Sato, Y. Nakasaka, K. Nagaoka, Kinetics of ammonia synthesis over Ru/Pr_2O_3, Journal of the Taiwan Institute of Chemical Engineers, 105 (2019), pp. 50-56.

[3] K. Sato, S. Miyahara, K. Tsujimaru, Y. Wada, T. Toriyama, T. Yamamoto, S. Matsumura, K. Inazu, H. Mori, T. Iwasa, T. Taketsugu, K. Nagaoka, Barium Oxide Encapsulating Cobalt Nanoparticles Supported on Magnesium Oxide: Active Non-noble Metal Catalyst for Ammonia Synthesis under Mild Reaction Conditions, 11 (2021), pp. 13050-13061.

[4] S. Hargen, R. Barfod, R. Fehrmann, C.H.Jacobsen, H. Teunissen, I. Chorkendorff, Ammonia synthesis with barium-promoted iron-cobalt alloys supported on carbon., J. Catal., 214 (2003),pp. 327-335.

[5] M. Kitano, Y. Inoue, M. Sasase, K. Kishida, Y. Kobayashi, K. Nishiyama, T. Tada, S. Kawamura, T. Yamada, M. Hara, H. Hosono, Self-organized Ruthenium-Barium Core- Shell Nanoparticles on a Mesoporous Calcium Amide Matrix for Efficient Low-Temperature Ammonia Synthesis, Angewandte Chemie International Edition, 57 (2018), pp. 2648-2652.

[6] M. Kitano, J. Kujirai, K. Ogasawara, S. Matsuishi, T. Tada, H. Abe, Y. Niwa, H. Hosono, Low-Temperature Synthesis of Perovskite Oxynitride-Hydrides as Ammonia Synthesis Catalysts, Journal of the American Chemical Society, 141 (51) (2019), pp. 20344-20353.

[7] Y. Inoue, M. Kitano, M. Tokunari, T. Taniguchi, K. Ooya, H. Abe, Y. Niwa, M. Sasae, M. Hara, H. Hosono, Direct Activation of Cobalt Catalyst by $12CaO \cdot 7Al_2O_3$ Electride for Ammonia Synthesis, ACS Sustainable Chem. Eng., (2019), pp. 2648-2652.

[8] W. Gao, P. Wang, J. Guo, F. Cheng, T. He, Q. Wang, G. Wu, P. Chen, Barium Hydride-Mediated Nitrogen Transfer and Hydrogenation for Ammonia Synthesis: A Case Study of Cobalt, ACS Catal., 7 (2017), pp. 3654.

[9] X. Wang, X. Peng, W. Chen, G. Liu, A. Zheng, L. Zheng, J. Ni, C. Au, L. Jiang, Insight into dynamic and steady state active sites for nitrogen activation to ammonia by cobalt-based catalysts, Nature Communication, 11 (2020), pp. 653.

[10] Y. Gong, J. Wu, M. Kitano, J. Wang, T. N. Ye, Y. Kobayashi, K. Kishida, H. Abe, Y. Niwa, H. Yang, T. Tada, H. Hosono, Ternary intermetallic LaCoSi as a catalyst for N_2 activation, Nature Catalyst, 1 (2018), pp. 178-185.

[11] R. Kojima, H. Enomoto, M. Muhler, K. Aika, Cesium-promoted rthenium catalysts supported on alumina for ammonia synthesis, Applied Catalysis A: General, 246 (2) (2003), pp. 311-322.

[12] T. N. Ye, S. W. Park, Y. La, J. Wu, M. Sasae, M. Kitano, H. Hosono, Dissociative and Associative Concerted Mechanism for Ammonia Synthesis over Co-Based Catalyst, Journal of the American Chemical Society, 143 (32) (2021),pp. 12857-12866.

[13] Y. Tang, Y. Kobayashi, N. Masuda, Y. Uchida, H. Okamoto, T. Kageyama, S. Hosokawa, F. loyer, K. Mitsukawa, K. Yamanaka, Y. Tamenori, Metal-Dependent Support Effect of Oxyhydride-Supported Ru, Fe, Co, Catalysts for Ammonia Synthesis, Advanced Energy Materials, 8 (2018), pp. 1801772.